Investigation on the Discharge Arc Behavior of a Segmented Anode Pulsed Plasma Thruster

IEPC-2019-A-497

Presented at the 36th International Electric Propulsion Conference
University of Vienna • Vienna, Austria
September 15-20, 2019

Zhe Zhang[1], William Yeong Liang Ling[2], Haibin Tang[3]
Beihang University, Beijing 100191, China

Abstract: The low performance of Ablative pulsed plasma thrusters (APPTs) has been a drawback for decades. This is the main challenge for APPTs to be implanted on small satellites and spacecrafts. An asymmetrical anode schematic was proposed recently showing to enhance the performance of APPTs. It is using an interrupted anode (named segmented anode) to enhance the discharge and ablation process. The improved asymmetrical electrodes structure can potentially enable promising applications in future space tasks. In the present work, we aim to understand the physical processes behind this asymmetrical discharge mode, experiments using an ultra-high-speed camera and narrow bandpass filters were conducted with both normal parallel-plate electrodes and a segmented anode on an experimental APPT. Large amount of speed images were taken regarding the light emission from C^+, neutral C_2, and broadband emission reveal the evolution of the plasma morphology on an APPT with a segmented anode. The high speed data indicates that, the arc morphology of the segmented anode APPT with asymmetric electrodes has a restricted arc attachment point, possibly resulting in stronger arc current density at the anode corner. The further effect of the arc attachment point is to increase the ionization rate and the ablation mass. The arc restriction effect and the segmented electric field fundamentally changes the physical process behind APPT operation, meaning that the improvements should also be applicable to other APPT designs.

Keyword: Ablative pulsed plasma thrusters, segmented anode, arc behaviour, arc propagation.

I.Introduction

On January 21st 2019 at the beginning of this year, China successfully launched two satellites named "Spectrum01/02". These two satellites are equipped with ablative pulsed plasma thrusters (APPTs) as the primary propulsion system for orbital control. APPTs exhibit some advantages over most other electric propulsion systems, such as a flexible power consumption level, low operational risk, and low development cost, making them a competitive electric thruster for CubeSat applications[1,2,3]. However, the low efficiency and small μN-level thrust has long remained a performance problem to be solved [4,5].

Generally, the operation process of an APPT can be mainly divided into ablation, ionization, and acceleration[6]. The thrust is generated by the kA-level self-induced electromagnetic, the Lorentz force will accelerate the plasma and then produce thrust. However, these processes involves in several physical phenomena (ionization[7], ablation[8], plasma acceleration[9], and plasma propagation[10]) and coupled with strong electromagnetic interfere during the μs-level

[1] Post-doctoral researcher, School of Instrumentation and Optoelectronic Engineering, zhangzheplasma@buaa.edu.cn
[2] Associate professor, School of Aerospace, wling@bit.edu.cn
[3] Professor, School of Space and Environment, thb@buaa.edu.cn

discharge. Unlike the most stationary thrusters such as ion and Hall thrusters[11,12,13], APPT plasma have a complex composition with multiple species (C, C^+, F, F^+, C_2, CF, CF_2, etc.)[14]. Thus the physical mechanisms and interactions that occur inside the APPT discharge channel (the volume between the electrodes) are very challenging to study[15].

Recently, a asymmetrical segmented anode schematic was proposed to increase the performance parameters of APPTs while using the same input energy[16,17]. The preliminary results show that the main discharge arc current density and the propellant mass ablation was enhanced using the segmented anode schematic. However, it is still necessary to understand the plasma distribution and the behaviour of the discharge arc when a segmented anode is used with an APPT.

This work studies the physical mechanism and discharge arc behaviour during the 10 μs discharge of a recently reported segmented anode APPT[5]. We aim to demonstrate the physical processes and discharge arc propagation morphology of a segmented anode 20 J APPT with a rectangular geometry. To gain a deeper understanding of the performance improvement associated with a segmented anode, an experimental high-speed camera imagery system combined with optical filters was constructed, and long-duration imagery was obtained. An APPT with a continuous normal anode and a segmented anode were studied, with a focus on the differences in the plasma morphology, arc luminosity, and plasma propagation processes.

II.Experimental apparatus

The thruster, vacuum facility, and high speed imaging system is introduced in this section. All comparison experiments used a single control variable settings.

A. Asymmetrical APPT and vacuum system

The thruster used in our experiment is a breech-fed experimental APPT. The asymmetrical design is on the anode schematic. Unlike the normal uninterrupted anode, the asymmetrical electrode is the anode segmented by a ceramic segment (machineable fluorophlogopite-based glass ceramic), which makes the copper upstream and downstream segments insulated from each other at the surface. At the same time, the upstream and downstream segments were electrically connected at the bottom. A photograph of the asymmetrical segmented anode APPT as shown in Figure 1. The electrode was 15 mm for both normal and segmented anode; for the segmented anode layout, the ceramic segment (2 mm in length) located 4 mm from the propellant surface, followed by a downstream segment that brought the total length to 15 mm. The discharge gap between the electrodes was 20 mm and the width was 18 mm.

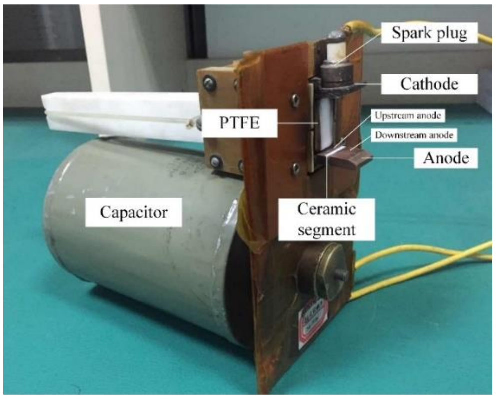

Figure 1. A photograph of the asymmetrical APPT

The APPT experiments were carried out in a vacuum chamber with a diameter of 0.8 m and a length of 1.8 m. The chamber was equipped with a DIS-500 rotary pump and a CRYO-U 12HSP cryogenic pump. The base pressure was less than 3×10^{-3} Pa before experiments.

B. Ultra-high-speed camera and optical filters

Due to the extremely short duration (10μs level) of the operation process of APPT, it is quite hard to distinguish the plasma propagation process and component during the operation. In this work, an ultra-high-speed camera (Invisible

Vision, Ultra UHSi 24) was used to study the working mechanism through the arc morphology, plasma propagation, and restrike phenomenon. This is a high-speed framing camera with a 16 megapixel GigE-linked CCD that can take a series of 24 images at a maximum frame rate of 200 million frames per second (fps). This makes it possible to clearly demonstrate the operation process and plasma development behaviour during the whole discharge process inside the electrodes.

In our experiments, images were taken at a frame rate of 1 to 10 million fps and with an exposure time of 100 ns and gain of 100. 12 images were taken in one APPT firing. The delay between each high-speed image was 0.6 μs with a total capture time of 7.2 μs, meaning that 12 images were taken during operation process of the APPT. When it to refers the discharge period, the high speed images correspond to the first to the third half cycle in one discharge. In the first to third half cycle, phenomena such as restrikes, plasma propagation, and plasma acceleration have already taken effect and based on the results in reference [4], most of the energy (~85%) is consumed in these stages.

Two wavelengths were selected for imaging in addition to broadband light emission: 514.5 nm emission from the neutral C_2 and 426.8 nm emission from C^+ ions. Narrow bandpass filters with a diameter of 70 mm (Shenzhen nano macro photoelectric technology co., LTD) were used to isolate these wavelengths. These bandpass filters could be used to observe single component behavior of the plasma. The filters have central wavelengths of 514.5±2 nm and 426.8±2 nm and a full-width-half-maximum of 10±2 nm. The wavelength of the two bandpass filters are shown in Figure 2. Long-duration images with these filters were also captured using a commercial Nikon D750 camera with a Nikon lens AF-S 70-200mm f/2.8E. 514.5 nm emission from neutral C^2 and 426.8 nm from C^+ ions were isolated using narrow bandpass filters (Shenzhen Nano Macro Photoelectric Technology Co., Ltd.). Bandpass filters with a diameter of 70 mm were placed on the camera lens; the filters have central wavelengths of 514.5±2 nm and 426.8±2 nm and a full-width-half-maximum of 10±2 nm.

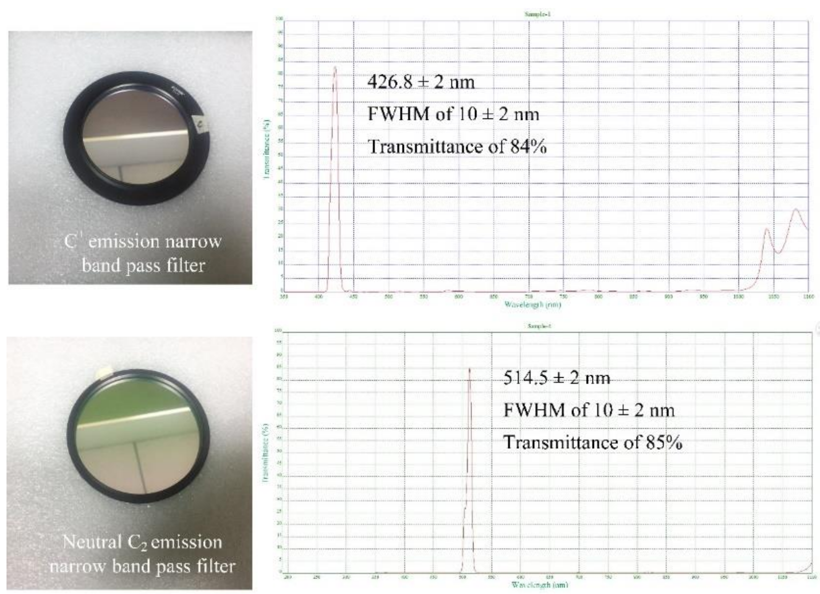

Figure 2. Bandpass filters.

As shown in Figure 3, the entire high-speed imaging system consisted of an ultra-high-speed camera (Ultra UHSi 24), a signal generator (SRS DG535), an oscilloscope (Tek DPO3014), a high-voltage probe (Tek P5100) to detect the spark plug trigger, a high-voltage probe (Tek P5200) to detect the APPT discharge voltage, a Rogowski coil, and a control computer[18]. One of the oscilloscope channel is used to record the spark plug signal, this signal was used as the trigger to input a signal into the signal generator DG535. The signal generator will then output a standard 5V TTL signal into both the high-speed camera and oscilloscope. Through this signal, the camera shutter will be triggered and the initial triggering time of the camera shutter would also be recorded. This allows us to compare the first high speed image time to the discharge initial time. To protect the high speed camera from electromagnetic interference, the spark plug signal and the high-speed camera input signal were isolated from each other. The camera's control software was used to change the camera's shutter delay to coincide with the onset of the APPT discharge (based on the discharge voltage and current curves). Finally, we can measure the discharge voltage and current, spark plug signal, and shutter timing of the 5V TTL signal simultaneously in one discharge using the oscilloscope.

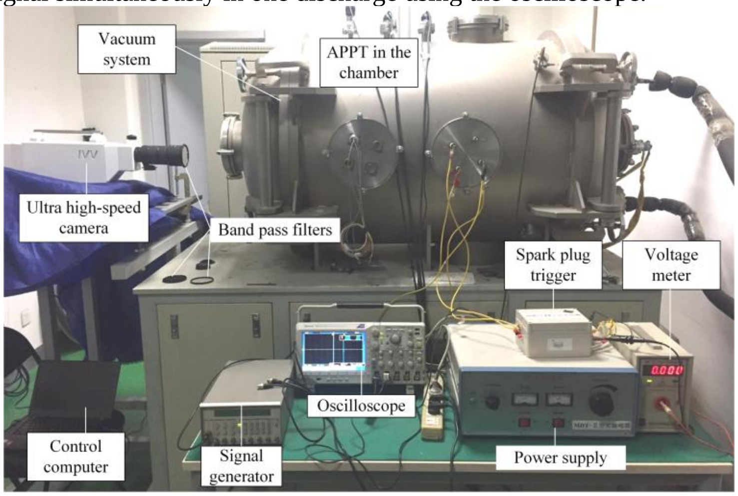

Figure 3. Photography of the high speed image system

III.Results and discussion

C. Long duration images for asymmetrical APPT and normal APPT

The APPT was operated under an initial discharge voltage of 1.8 kV (16.2 J) and discharge current of 19 kA. An asymmetrical segmented anode and a normal anode were tested under the same experimental settings. Commercial camera equipped with narrow bandpass filters were used to capture the images for two wavelengths 514.5 nm emission from the neutral C_2 and 426.8 nm emission from C^+ ions. In addition, broadband images for all light emissions were also recorded as the visual aid to to reveal difference between asymmetrical and normal APPTs.

Various long duration side-view images for normal and segmented anode APPT operation are shown in the three figures below. Figure 4, Figure 5, and Figure 6 shows the broadband emission, C^+ ions emission, C_2 emission, respectively. In all of the three figures, (a) stands for normal anode and (b) stands for segmented anode. The images were captured with an exposure time (2 s) far greater than the discharge time of ~10 μs; this presents a composite of the entire discharge process in a single image. Since the exposure time (shutter open to shutter close time) is several orders of magnitude longer than the PPT discharge time, the accuracy of the trigger time was not crucial. The entirety of the discharge emission could always be captured since the exposure time (2s) is much longer than the discharge duration (10μs).

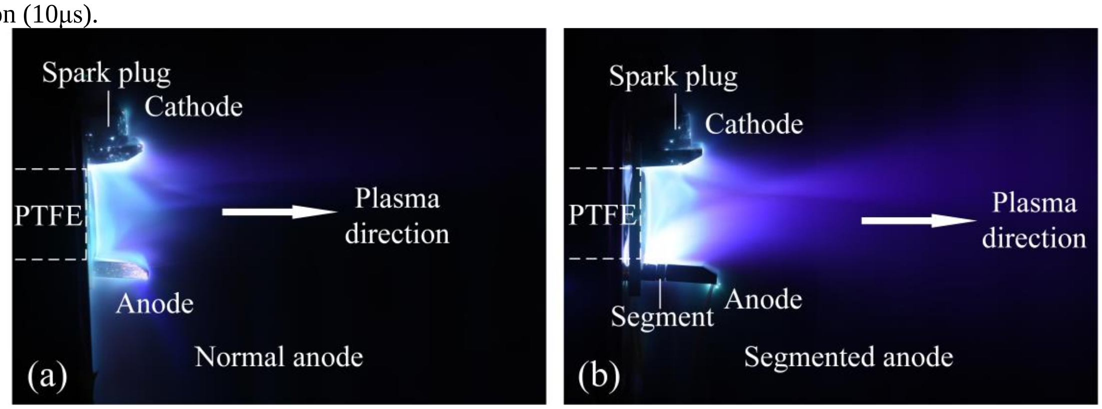

Figure 4. Broadband emission for (a) normal anode and (b) segmented anode APPT.

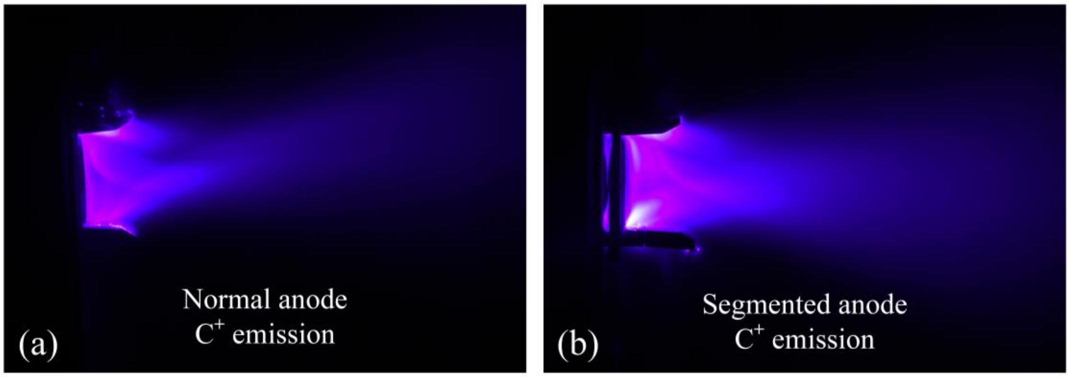

Figure 5. C^+ ions emission for (a) normal anode and (b) segmented anode APPT.

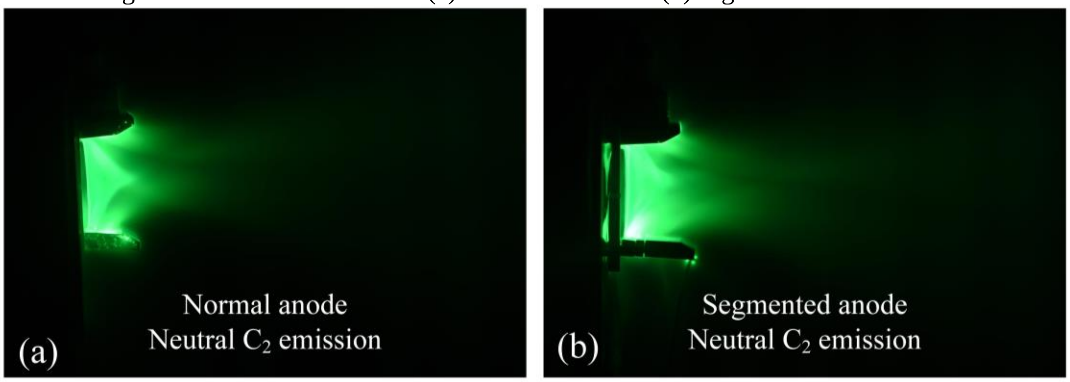

Figure 6. C_2 emission for (a) normal anode and (b) segmented anode APPT.

Clear differences between normal and segmented anode PPTs could be observed in the figures above. Comparing the broadband emission in Figure 4 (a) and (b), the luminosity pattern is brighter for the segmented anode PPT than that of the normal anode PPT. The band originating from the upstream segment also never appears in the conventional normal anode PPT. The component of this bright band is still unknown, since it appears in both C^+ emissions and C_2 emissions. The general structure of the long-duration images is very repeatable. The bright band near the segment anode is always present. When comparing the C^+ emission in Figure 5 (a) and (b), there is a significant bright section in the segmented anode PPT at the corner of the anode upstream location. This bright part locates before the ceramic insulator at the segmented anode upstream. Which indicates that the segmented anode schematic may enhance the current density and the ionization rate at this corner. When comparing the neutral C_2 emission in Figure 6 (a) and (b), there is also a brightness pattern distributed at the upstream before the ceramic in the images of segmented anode APPT. This is because the segmented anode PPT's arc migration is restricted before the ceramic segment, resulting in the discharge arc at the corner being better resolved. The restricted arc would increase the local temperature and energy intensity before at the upstream, and further increase the ablation mass for the segmented anode APPT.

D. High speed images

The shutter initial timing of the high speed camera was recorded regarding the discharge process of the APPT (as shown in Figure 7). Both the segmented anode and normal anode APPT were operated at an initial discharge voltage of 1800 V (16.2 J). The discharge curves have good repeatability.

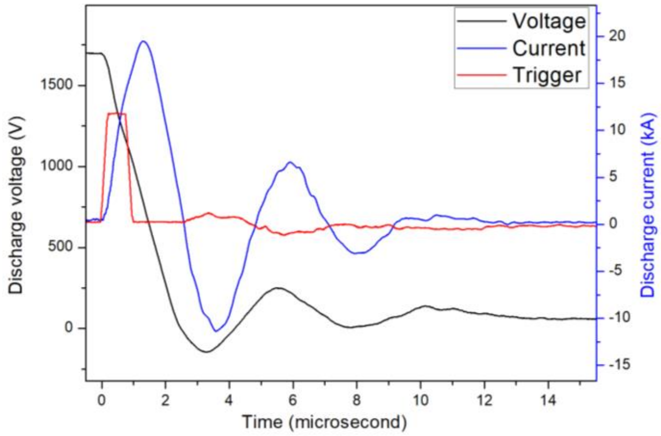

Figure 7. Discharge currents of normal and segmented anode APPTs with the ultra-high-speed camera's shutter timings.

High speed images for normal and segmented anode PPTs are compared in Figures 8 – 10. Locations and geometries of the cathode, anode, ceramic segment, and PTFE are shown in these images using dotted lines. The camera was set with f/5.6 and a gain of 100. Figure 8 shows the broadband light emission with no filter on the camera lens; Figure 9 is the high speed images from 426 nm emission from C^+ ions; Figure 10 shows the 514 nm emission from neutral C_2 with f/5.6 and a gain of 100. For each emissions were repeated at least 5 times to secure the discharge repeatability. In the figures below, an initial discharge voltage of 1800 V (with highest luminosity) were choose to best highlight the arc morphology and PPT working process.

As can be seen in Figure 8, there is an arc travelling phenomenon during the whole discharge process for the normal anode APPT. At the initial time, the arc shape appears a clear difference. The segmented anode APPT has a "I" shape along the PTFE surface, while the normal anode APPT has a "L" shape along the PTFE and the anode surface. This indicates initial discharge for the normal anode APPT is more diffuse over the segmented anode APPT. With the time developing, the arc of the normal anode APPT travels to the downstream towards the thruster exit due to the thermal expansion. As opposed to this, the segmented anode APPT has a quite stable arc attachment point due to the ceramic insulator at the upstream. This ceramic segment restricts the arc at the anode corner and improves the further ionization at the first and second half period of discharge. The restriction enhance the ionization analysis has a clear evidence in Figure 8 (b) from 2.4 to 6 μs.

From Figure 9, the C^+ ions generation and propagation process is demonstrated. There are significant differences in the plasma morphology and plasma luminescence intensity of the two schematic APPTs. For the main discharge process (0 to 2.4 μs), the C^+ ion emission of the segmented anode APPT is much higher than that of the normal anode APPT. This means that the segmented anode APPT exhibits a higher degree of ionization than the normal anode APPT during the main discharge process. For the restrike process (3.6 μs to 6 μs), the C^+ ions morphology, density and location are also appears clear differences from the normal anode APPT. The ion generation location is at the upstream near attachment point discussed in Figure 8 for the segmented anode APPT. Which verifies that the segmented anode schematic restricted arc and keept ionizating during the second to third period of the discharge.

For the neutral C_2 emission in Figure 10, during the main discharge period (0 to 2.4 μs), the arc morphology of the segmented anode APPT is similar to the normal anode APPT. However, during the arc propagation process (3.6 to 6 μs), the arc morphology of the segmented anode APPT deviates significantly from the normal anode PPT. Due to thermal expansion, the arc moves downstream after the main discharge period; this can be called downstream arc migration. However, differences appear in the attachment points depending on the anode type. The segmented anode APPT's arc migration is restricted by the ceramic segment. However, the attachment point of the normal anode PPT continually travels downstream along the anode. A stable upstream attachment point on the anode will restrict the arc nearer to the propellant surface. This may promote ionization and stabilizes the discharge arc morphology.

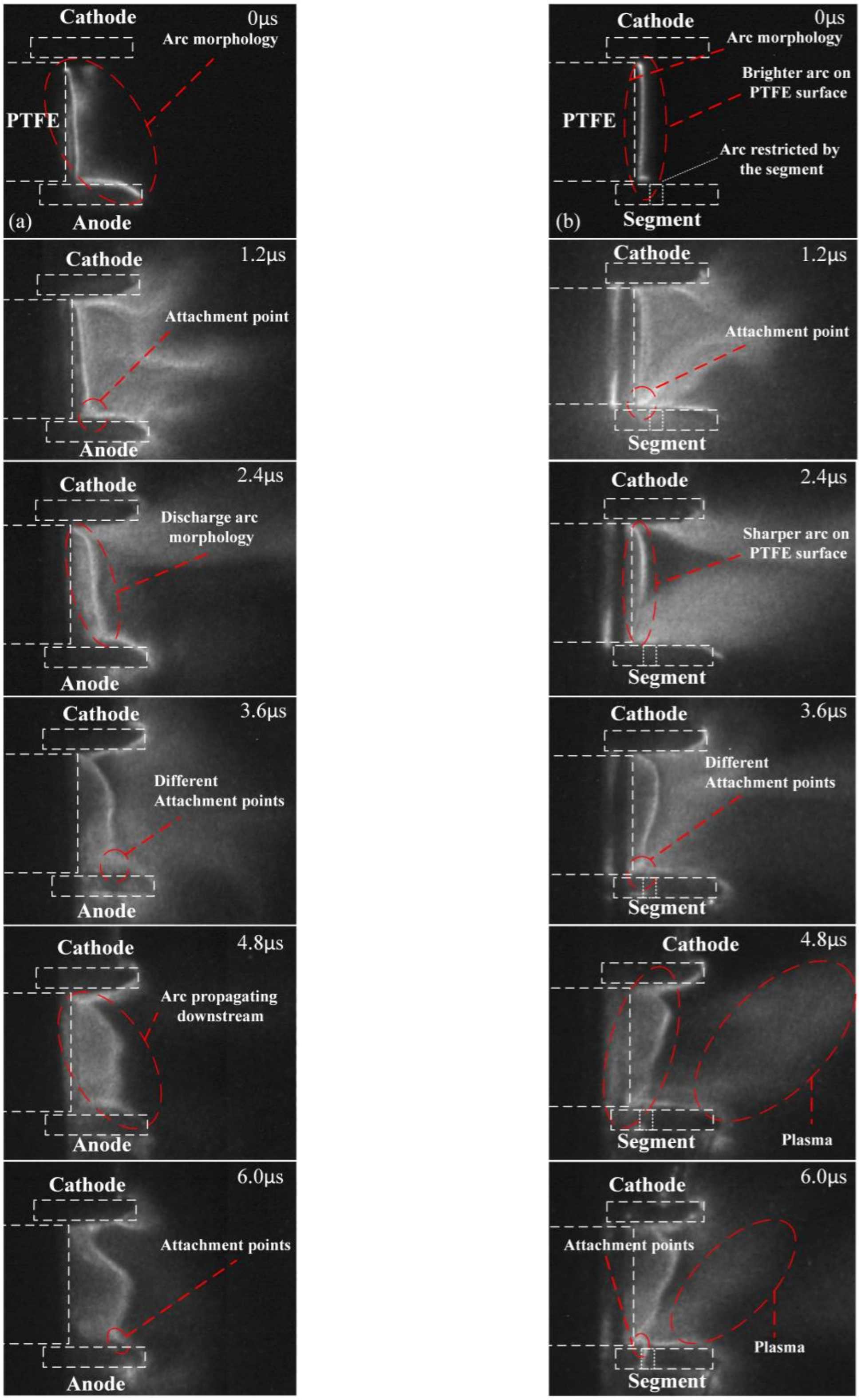

(a) Broadband emission for normal anode APPT (b) Broadband emission for segmented anode APPT

Figure 8. High speed images with broadband emission for normal and segmented anode APPT[18].

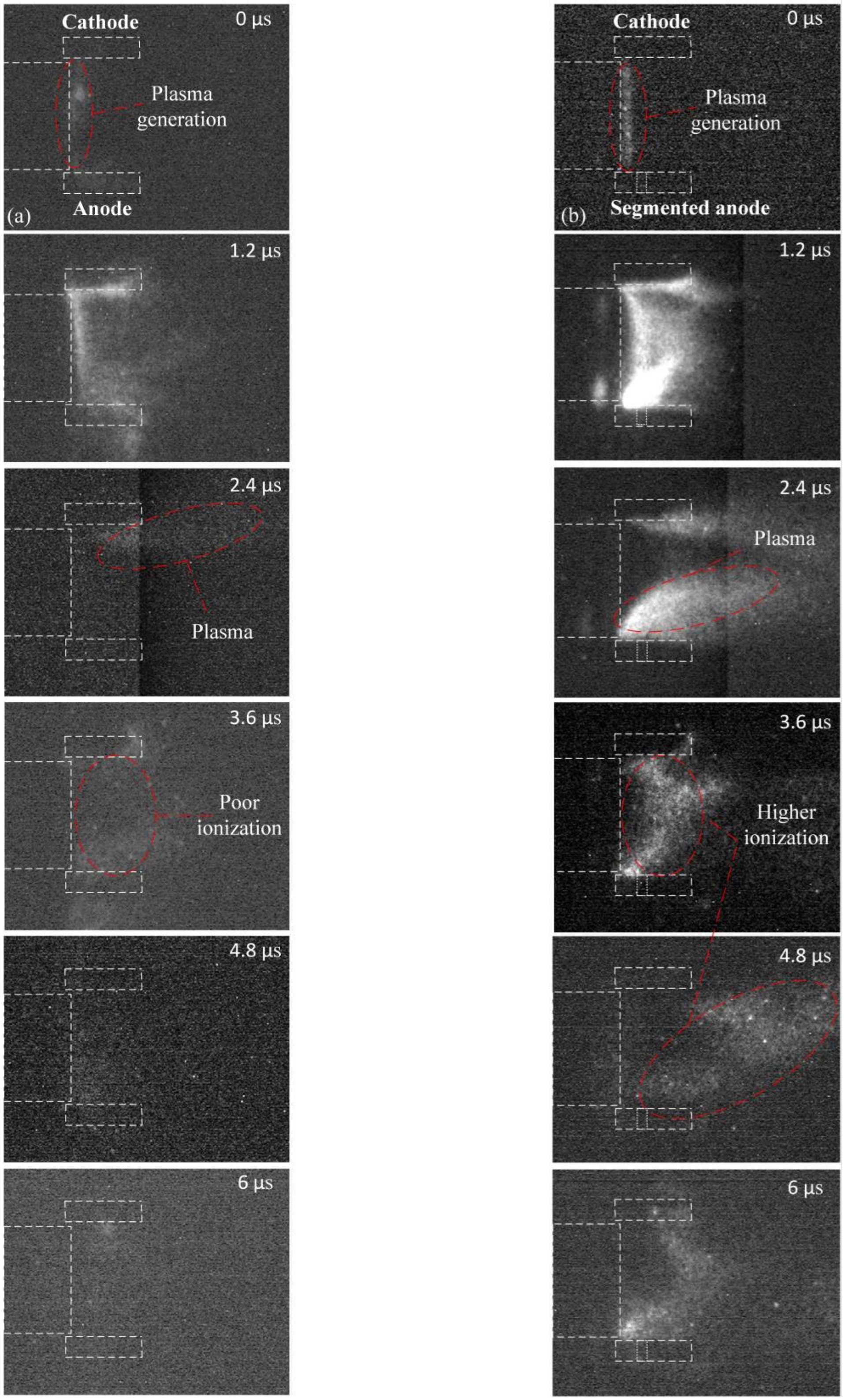

(a) Broadband emission for normal anode APPT (b) Broadband emission for segmented anode APPT

Figure 9. High speed images with C^+ ions emission for normal and segmented anode APPT[18].

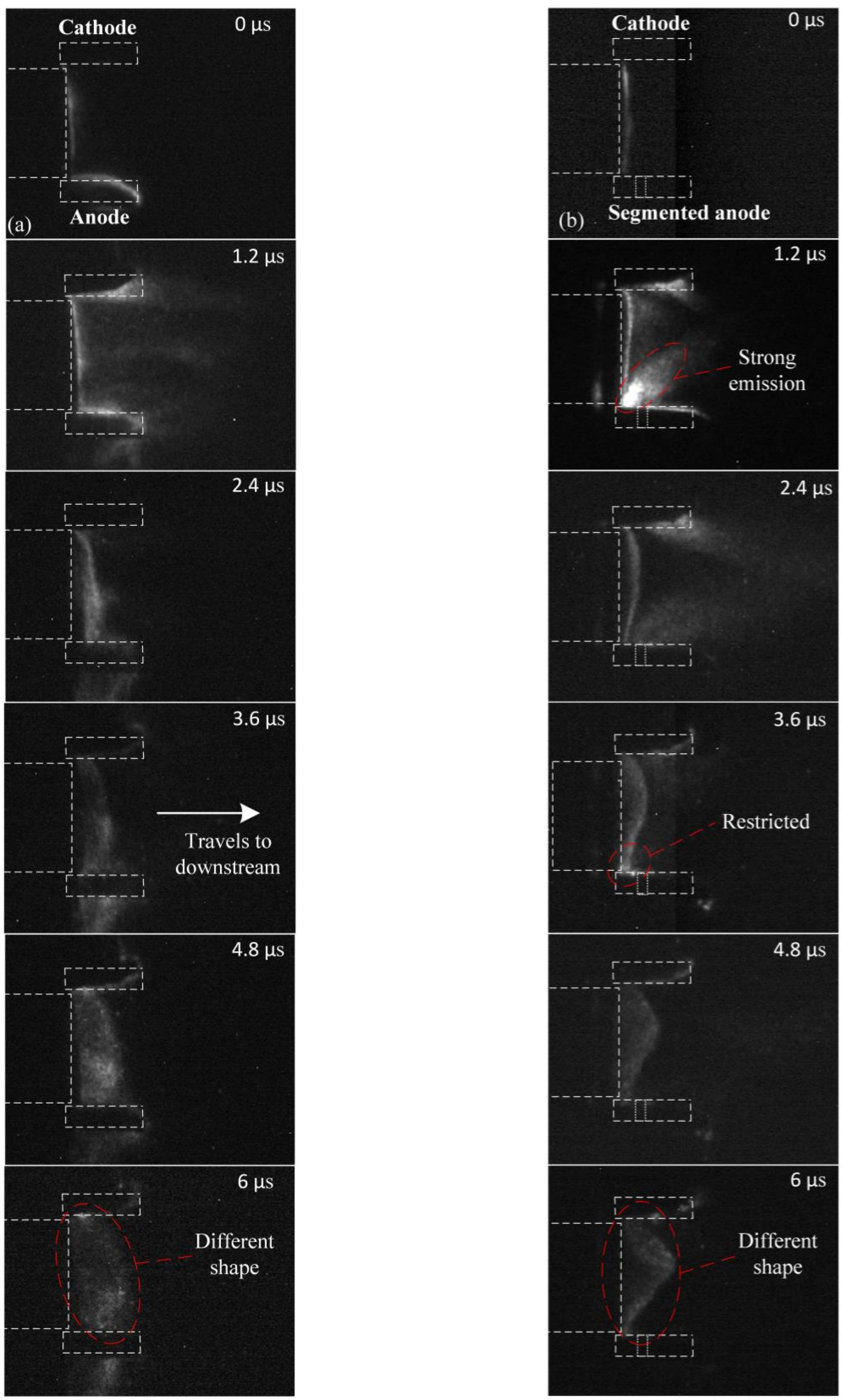

(a) Neutral C_2 emission for normal anode APPT (b) Neutral C_2 emission for segmented anode APPT

Figure 10. High speed images with neutral C_2 emission for normal and segmented anode APPT[18].

IV.Conclusion

This high speed imaging experimental research studies the physical mechanism behind the performance enhancement of asymmetrical segmented anode APPT. The relationship between the performance enhancement and discharge arc behavior was studied in this work. In addition, the physical mechanism behind the operation of an APPT with a segmented electrode is also identified using the high-speed imaging technology. The presented data confirms that a segmented anode positively alters the discharge arc morphology.

The physical mechanism of the performance enhancement of the segmented anode PPT was found to be the arc restriction effect. During the whole discharge process, the arc was restricted at the upstream segment before the ceramic segment. Thus, during the entire discharge process, the segmented anode PPT has a stable discharge arc "attachment point" on the anode corner near the PTFE surface, which may result in greater propellant mass ablation and ionization. The C^+ emission of a segmented anode PPT was found to be stronger and has a formation position nearer to the anode corner.

The improvement brought by this asymmetrical schematic is a fundamentally optimization, which could be easily applied to almost all existing PPT designs. This paper gives us a deeper understanding of the physical mechanisms behind this asymmetric electrode APPT, further quantitative data such as the ionization rate, the effect of the upstream and downstream segment lengths, and various component densities will be further studied in the future. These will possibly aid in more advanced optimization of this asymmetric electrode structure.

Acknowledgement

This work was supported by the National Natural Science Foundation of China (Grant No. 11872093).

References

[1] Burton R L, Turchi P J, Journal of Propulsion and Power, 14(5), 716-735, 1998.
[2] Jahn R G, in Physics of Electric Propulsion, (McGraw-Hill, New York, 1968), Chap. 9.
[3] Levchenko I, Bazaka K, Ding Y, Raitses Y, et al. Space micropropulsion systems for Cubesats and small satellites: From proximate targets to furthermost frontiers. Applied Physics Reviews, 5(1), 011104, 2018.
[4] Koizumi H, Noji R, Komurasaki K, Arakawa Y, Plasma acceleration processes in an ablative pulsed plasma thruster, Physics of Plasmas, 14(3), 033506-033506-10, 2007.
[5] Zhang Z, Ling W Y L, Tang H, Cao J, Liu X, Wang N, Characterization and optimization of ablative pulsed plasma thrusters, Review of Modern Plasma Physics, 3(5), 2019, DOI: 10.1007/s41614-019-0027-z
[6] Choueiri E Y, A critical history of electric propulsion: The first 50 years (1906-1956). Journal of Propulsion and Power, 20(2), 193-203, 2004.
[7] Schönherr T, Nees F, Arakawa Y, Komurasaki K, Herdrich G, Physics of Plasmas, 20(3), 033503(1-8), 2013.
[8] Yang L, Liu X, Wu Z, Wang N F, Applied Physics Letters, 104(8), 084102-084102-4, 2014.
[9] Koizumi H, Noji R, Komurasaki K, Arakawa Y, Plasma acceleration processes in an ablative pulsed plasma thruster, Physics of Plasmas, 14(3), 033506-033506-10, 2007.
[10]Schönherr T, Komurasaki K, Herdrich G, World Academy of Science, Engineering and Technology, 563-569, 2011.
[11] Dan M G, Katz I, Fundamentals of Electric Propulsion: Ion and Hall Thrusters, 2008.
[12] Zhang Z, Tang H B, Zhang Z, Cao S. A retarding potential analyzer design for keV-level ion thruster beams. Review of Scientific Instruments, 2016, 87(12):123510.
[13] Goebel D M, Katz I, Fundamentals of electric propulsion: ion and Hall thrusters, John Wiley & Sons, published in Hoboken, New Jersey, 2008.
[14] Rezaeiha A, Schönherr T. Review of worldwide activities in liquid-fed pulsed plasma thruster. Journal of Propulsion and Power, 30(2), 253-264, 2015.
[15] Schönherr T, Stein M, Komurasaki K, Herdrich G. Investigation of Discharge Arc Phenomena in Ablative PPT. IEPC-2015-79, Kobe, 2015.
[16] Zhang Z, Ren J X, Tang H B, Ling W Y L, York T M. An ablative pulsed plasma thruster with a segmented anode, Plasma Sources Science and Technology, 27(1), 2018.

[17] Zhang Z, Ren J, Tang H, Xu S, Ling W Y L, Cao J, Inter-electrode discharge of an ablative pulsed plasma thruster with asymmetric electrodes, Plasma sources science and technology, 27(12), 124003, 2018.
[18] Zhang Z, Ling W Y L, Ren J, Tang H, et al. The plasma morphology of an asymmetric electrode ablative pulsed plasma thruster, Plasma sources science and technology, 28(2), 025008, 2019.